Dynamics of the AlPdMn icosahedral phase

1993 J. Phys.: Condens. Matter 5 4945

(http://iopscience.iop.org/0953-8984/5/28/010)

J. Phys.: Condens. Matter 5 (1993) 4945–4966. Printed in the UK

Dynamics of the AlPdMn icosahedral phase

M de Boissieu†, M Boudard†‡, R Bellissent§, M Quilichini§, B Hennion§, R Currat‡, A I Goldman‖ and C Janot‡¶

† Laboratoire de Thermodynamique et Physico-Chimie Métallurgiques, UA CNRS 29, ENSEEG, BP 75, 38402, St Martin d'Hères Cédex, France

‡ Institut Laue–Langevin BP 156, 38042, Grenoble Cédex 9, France

§ Laboratoire Léon Brillouin, Centre d'Energie Nucléaire Saclay, 91 191 Gif sur Yvette Cédex, France

‖ Ames Laboratory, USDOE and Department of Physics and Astronomy, Iowa State University, Ames, IA 500011, USA

¶ Laboratoire de Cristallographie, CNRS, BP 166, 38042 Grenoble Cédex, France

Received 15 February 1993

Abstract. A centimetre-sized single grain of the perfect AlPdMn icosahedral phase was grown by slow cooling from the melt. It has been fully characterized to be of perfect icosahedral symmetry, i.e. without any frozen-in phason strain. The dynamical properties of this icosahedral phase have been studied by means of inelastic neutron scattering measurements on a triple-axis spectrometer. The response function $S(Q, \omega)$ was measured around several Bragg reflections and along the high-symmetry twofold, threefold and fivefold axes of the icosahedron. In the long-wavelength limit there are well defined phonons whose width is limited by the instrumental resolution. The isotropy of acoustic modes is verified and the corresponding sound velocities are in good agreement with ultrasonic measurements made on the same sample. At shorter wavelengths, gaps are expected. By analogy with 1D models and electron density of states calculations, the positions in reciprocal space where the strongest gaps are expected may be estimated. This defines a set of three main pseudo-Brillouin zones which are quasiperiodically stacked around each strong Bragg reflection chosen as the zone centre. In the limit of the instrumental resolution no gap could be detected, even when two branches crossed. Longitudinal and transverse modes become dispersionless for an energy equal to about 3 THz. A 4 THz optic branch is associated with the longitudinal mode. The energy width of the phonons is resolution limited for excitations below 2 THz but increases rapidly to reach a maximum value equal to 1 THz. For transverse modes propagating along two-, three- and fivefold axes this abrupt broadening is found to be isotropic and occurs for q lying between 0.4 and 0.7 Å^{-1}. This broadening is interpreted as being a consequence of a continuous distribution of dispersionless modes in the range 2–4.5 THz. Two main 'optic bands' centred on 3 and 4 THz may be defined in this region.

1. Introduction

The atomic structure of quasicrystals is now best understood via higher-dimensional crystallography. Periodicity is recovered in the higher-dimensional space and the structure may be described by a set of atomic surfaces decorating the periodic high-dimensional lattice (for recent reviews see [1] and [2] and for an introduction to the subject see [3]). The calculation of the dynamical response of quasicrystals remains difficult, however, since atomic surfaces are not point-like objects and the Bloch wave expansion is not an appropriate description of waves propagating in a quasilattice.

Several theoretical studies of the dynamical properties of quasicrystals have been performed, mainly on one-dimensional (1D) quasiperiodic chains [4–21] (for reviews see

0953-8984/93/284945+22$07.50

[22] and [30]), but also for two- and three-dimensional (3D) models using large unit cell periodic approximants [23–28]. The main features predicted for the one-dimensional case may be summarized as follows: in the long-wavelength limit, where the quasicrystal is described by a continuum, there is a linear dispersion relation; at shorter wavelength, the vibrational density of states exhibits a dense set of gaps arranged in a self-similar manner and wavefunctions are defined as 'critical', i.e. neither extended nor exponentially localized.

As may be expected, the situation is more complex when going to the 3D case. In the long-wavelength limit, there is still a linear dispersion relation, with isotropy imposed by the high symmetry of the icosahedral point group. For shorter wavelengths it is not yet clear whether states are localized or extended. Los *et al* [26] calculated the dispersion relation for various periodic approximants to the 3D Amman tiling. Their results show dispersion relations which are in some sense similar to the 1D case, although much more intricate. For instance, one may follow a transverse acoustic branch with a gap opening at each the Brillouin zone boundary crossing. The energy width of these gaps increases with the wavevector. As may be expected there are a large number of optic modes. Their density increases when the energy increases. When calculating the inverse participation ratio for this model, which is a measure of localization, only very high-energy modes show a high degree of localization while other modes are rather extended. Similar results were obtained by Hafner and Krajci for an AlZnMg atomic model [27]. In contrast, a calculation performed by Poussigue *et al* [28], for an AlMn quasicrystal model, seems to show that localization indeed occurs, even for relatively low-energy modes, leading to a broadening of the response function $S(Q, \omega)$. Finally, calculations carried out by Kasner *et al* [29], on a 3D atomic model with three different types of atom, show a rather smooth vibrational density of states without any gap.

Experimentally two icosahedral phases, of different atomic structures, were studied: i-AlLiCu [30, 31] and i-AlCuFE [32, 33]. The isotropy of acoustic modes has been confirmed in both samples, and was also observed in the cubic approximant R-AlLiCu phase. Dispersion relations were measured showing pseudo-zone boundaries. The comparison of higher-energy modes measured in both the icosahedral and the R-AlLiCu phase showed differences which are consistent with an enhanced degree of localization of these excitations in the icosahedral phase [31].

We present in this paper results of measurements performed on an AlPdMn single grain. The atomic structure of this icosahedral phase is similar to that of AlCuFe [34–36] but presents a different local order from the i-AlLiCu phase [37]. In section 2 we recall the basic notions concerning inelastic neutron scattering measurements. Predictions concerning the acoustic modes and the opening of gaps are discussed. In section 3 details of the instrumental configuration, data acquisition, and analysis are given. In section 4 we present the experimental results.

2. Measuring the phonon dispersion relation

We recall here the basic notions which are necessary to understand the inelastic neutron scattering measurements performed on a triple-axis instrument. Although this might seems trivial, we find it necessary to clarify the interpretation of experimental results.

In a triple-axis experiment a neutron with incident wavevector $\boldsymbol{k}_i$ is inelastically scattered into a solid angle $d\Omega$, with a final wavevector $\boldsymbol{k}_f$. The experimental quantity measured is the inelastic differential cross section which is related to the response function $S(\boldsymbol{Q}, \omega)$ by the relation [38]

$$d^2\sigma/d\Omega dE = (k_f/k_i)S(\boldsymbol{Q}, \omega) \tag{1}$$

where the momentum transfer $\boldsymbol{Q}$ is equal to $\boldsymbol{k}_f - \boldsymbol{k}_i$ and the energy E transferred to the sample is $\hbar\omega = (\hbar^2/2m)(k_i^2 - k_f^2)$. The response function is the double Fourier transform over time and space of the correlation function $G(\boldsymbol{R}, t)$.

Determining phonon dispersion relations consists of assigning each measured excitation to a given branch. This can only be handled in general for simple periodic structures with a few atoms in the unit cell [39]. For a periodic structure with n atoms in the unit cell the response function is a sum over the $3n$ modes:

$$S(\boldsymbol{Q}, \omega) = \sum_{j}^{\text{all modes}} S_j(\boldsymbol{Q}, \omega) \tag{2}$$

where j is the label of a given branch. For each branch the phonon wavevector corresponding to inelastic measurements is defined by the relation $\boldsymbol{q} = \boldsymbol{Q} - \boldsymbol{G}$, where $\boldsymbol{Q}$ is the momentum transfer and $\boldsymbol{G}$ is the position vector of the zone centre (Bragg peak) closest to $\boldsymbol{Q}$ in reciprocal space. In the harmonic approximation the response function is related to the inelastic structure factor by [39]

$$S_j(\boldsymbol{Q}, \omega) = \langle n(\omega) + \tfrac{1}{2} \pm \tfrac{1}{2}\rangle/\omega_j(\boldsymbol{q}) F_{\text{in}}(\boldsymbol{Q})\delta(\omega \pm \omega_j(\boldsymbol{q})). \tag{3}$$

The first term in angular brackets describes the phonon population at temperature T, with the upper and lower signs corresponding to phonon creation and annihilation respectively. The inelastic structure factor $F_{\text{in}}(\boldsymbol{Q})$ involves a sum taken over all atoms in the unit cell:

$$F_{\text{in}}(\boldsymbol{Q}) = \sum_k M_k^{-1/2} b_k \boldsymbol{e}_k^j(\boldsymbol{q}) \cdot \boldsymbol{Q} \exp(i\boldsymbol{Q} \cdot \boldsymbol{r}_k) \exp(-w) \tag{4}$$

where b_k is the scattering length of the atom k, $\boldsymbol{e}_k^j$ the polarization of the jth mode and $\boldsymbol{r}_k$ the position of the atom in the unit cell. For simple structures with only a few atoms in the unit cell, the contribution of the different branches may be easily distinguished by means of the scalar product $\boldsymbol{e}_k^j \cdot \boldsymbol{Q}$ in expression (4). For more complex structures (up to ten atoms) this is no longer true and the usual procedure is to compute the inelastic structure factor using a model and then look for places in reciprocal space where only a few modes have a significant, measurable, inelastic structure factor.

In general measured phonons do not have an infinite lifetime because of anharmonicity, interaction with defects, etc. This produces a broadening of the excitations which are no longer delta functions as in expression (3). This is taken into account by fitting the experimental constant-Q spectra with the response function of a damped harmonic oscillator convoluted with the instrumental resolution, which is a natural generalization of expression (3) [39]. As a result of the fit, phonon frequencies and inelastic structure factors are evaluated, together with the energy width which is related to the phonon lifetime.

For quasicrystal materials such a simple situation does not hold any longer. Unlike the case of incommensurate structures there is no underlying periodic structure which may be used as a guide for the description of the dispersion relations. Since the unit cell is infinite, the Brillouin zone shrinks to a point and there are an infinite number of modes. The only way to interpret data would thus be to compute the response function starting from a realistic atomic model and potential interactions, and compare it to experimental results.

This situation may seem depressing, but fortunately there are a few rules of thumb that may guide the measurement and their qualitative interpretation. In particular there are simple predictions concerning acoustic modes on one hand, and the location and energy width of gaps on the other hand.

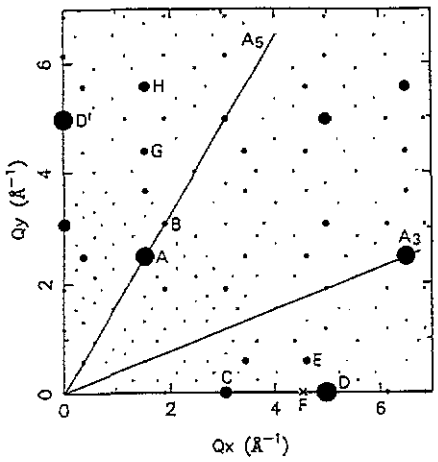

Figure 1. Twofold scattering plane of the AlPdMn icosahedral phase. The areas of the spots are proportional to the intensities calculated with the proposed model. Indices of labelled peaks are given in table 1.

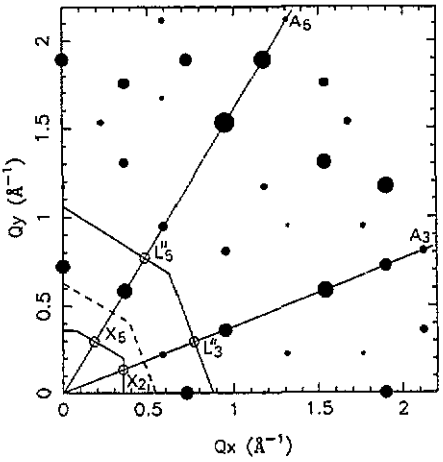

Figure 2. Twofold reciprocal plane showing the strongest 'mass' structure factor F_m (see text). The area of each spot is proportional to F_m. The trace on the twofold plane of the first three important Brillouin zone boundaries is indicated together with the labelling of important points. Corresponding indices are given in table 2. This set of pseudo-zone boundaries may be placed around each of the strong Bragg reflections of figure 1.

2.1. *Acoustic modes*

In the very long-wavelength limit ($|q| \to 0$), where the quasicrystal may be treated as a continuum, one expects to have well defined collective excitations. This is the only region where there is a direct link between the measured spectra and a single-phonon branch. Because of the high symmetry of the icosahedral point group there are only two different acoustic modes, one longitudinal and two degenerate transverse modes. In this region the dispersion relation is linear, with a slope related to sound velocities, and given by

$$\omega_{T(L)}(q) = v_{T(L)} \cdot |q| \tag{5}$$

where T and L stand for transverse and longitudinal modes.

Performing a Taylor expansion in expression (4), it can be shown that the response function of acoustic modes can be written

$$S_{T(L)}(Q,\omega) = \langle n(\omega) + \tfrac{1}{2} \pm \tfrac{1}{2} \rangle / \omega_{T(L)}(q)(e_{T(L)} \cdot Q)^2 \cdot F_{el}^2(G) \cdot \delta(\omega \pm \omega_{T(L)}(q)) \tag{6}$$

where $e_{T(L)}$ is a polarization vector orthogonal (parallel) to the phonon wavevector q corresponding to transverse and longitudinal polarization and $F_{el}(G)$ is the elastic structure factor of the quasicrystalline structure. The important part in this relation is the usual $(e_{T(L)} \cdot Q)^2 |F_{el}(G)|^2$ factor which tells us that acoustic modes should be measured at high momentum transfer value and close to a strong Bragg peak in order to have the largest possible signal. For a general relative orientation of q and Q, both the transverse and the longitudinal modes will give a contribution to the response function $S(Q,\omega)$, but, as it is usual, this scalar product allows us to choose regions in reciprocal space where only one acoustic mode will contribute.

Figure 1 shows the experimental scattering reciprocal space plane. This is a twofold plane which contains all the symmetry axes of interest, i.e. two-, three-, and fivefold axes. Some of the strongest spots are labelled and their corresponding indices are given in table 1 [41]. Although, in principle, there are Bragg reflections everywhere in reciprocal space, only a finite number of them have a measurable intensity. As a consequence of relation (6), measurements were performed close to Bragg reflections, A, B, C, D, E, D', G, and H: well defined acoustic modes are expected close to these peaks.

Table 1. Labels and indices of some strong reflections shown in figure 1. Indices are given following the scheme of Cahn *et al* [42] and in the primitive unit cell. In figure 1 D' is a twofold reflection equivalent to D.

Label	N	M	M_u	h/h'	k/k'	l/l'	n_1	n_2	n_3	n_4	n_5	n_6	Q_{par} (Å^{-1})
A	18	29	12	1/2	2/3	0/0	1	2	1	−1	1	1	2.917
B	28	44	12	2/2	2/4	0/0	1	3	1	−1	1	1	3.606
C	20	32	30	2/4	0/0	0/0	1	2	0	−1	2	0	3.068
D	52	84	30	4/6	0/0	0/0	2	3	0	−2	3	0	4.963
E	46	73	60	3/6	0/1	0/0	2	3	0	−1	3	0	4.638
G	46	73	60	1/2	4/5	0/0	2	3	1	−2	2	1	4.638
H	70	113	60	1/2	4/7	0/0	2	4	1	−2	3	1	5.757

2.2. *Gap opening*

Due to the lack of periodicity there are, in principle, an infinite number of gaps opening in the dispersion relation. Following the procedure used for the 1D case [11, 13, 18] and for electronic properties [40, 41], one can however estimate where the strongest gaps should be located for the AlPdMn icosahedral phase. For electronic properties this corresponds to the weakly perturbated free electron model, whereas for phonons the description corresponds to a weak perturbation of the monoatomic Bravais lattice.

Dynamical properties of the 1D Fibonnacci chain have been widely studied, and we first recall the basic results obtained when a perturbative approach is applied [11, 13, 18]. The Fibonnacci chain is a quasiperiodic stacking of two segments, a long and a short one. The phonon dispersion relation may be described starting from the dispersion relation of the monoatomic chain. The quasiperiodicity is introduced as a weak perturbation in a very crude first approximation. This, however, allows us to locate all important gaps in the pseudo-dispersion relation. A gap opening results from the reflection of the phonon wave on a Bragg plane. As a consequence, if a gap opens at $G + q$, where G is a vector of the quasiperiodic reciprocal lattice, then $2q$ is also a vector of this reciprocal lattice. It can also be shown that the energy gap width is proportional to $F(2q)$, where F is the structure factor of the 1D quasiperiodic chain. Using these relations one can then easily locate the position q of the few important gaps by computing the structure factor $F(2q)$. The locations of these gaps define pseudo-Brillouin zone boundaries. Each time the acoustic branch crosses such a special point there is a gap opening, the dispersion relation presenting a horizontal slope. Because of inflation properties of the Fibonnacci chain there is a series of gaps whose position scales with τ, the golden mean, and whose energy width increases [11, 13, 18]. In this perturbative approach the 'envelope' of the dispersion relation is that of the monoatomic periodic chain, which implies that the upper value of $2q$ to be considered in the calculation is given by the period of monoatomic chain.

It is interesting to compare these results to the response function calculation performed by Benoit *et al* (see for instance their figures 4, 5, 6 in [19]): this is a simulation of a 1D inelastic neutron scattering experiment and it has been found to be very helpful in 3D data interpretations. At first glance the situation seems to be much more complicated. However the positions and relative intensities of the gaps are well predicted. Close to strong Bragg peaks there are well defined acoustic modes, whose dispersion relation shows gaps. Only the two or three strongest gaps are important and would be 'measurable' in this case. One should note however that in the high-energy region, there are many optical modes whose presence cannot be accounted for by this simple perturbative approach.

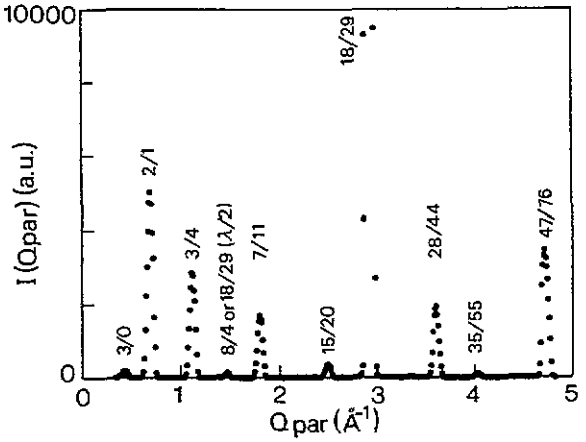

Figure 3. Elastic q scan along a fivefold axis. All peaks belong to the icosahedral phase. Some of them are indexed in the scheme of Cahn *et al* [42].

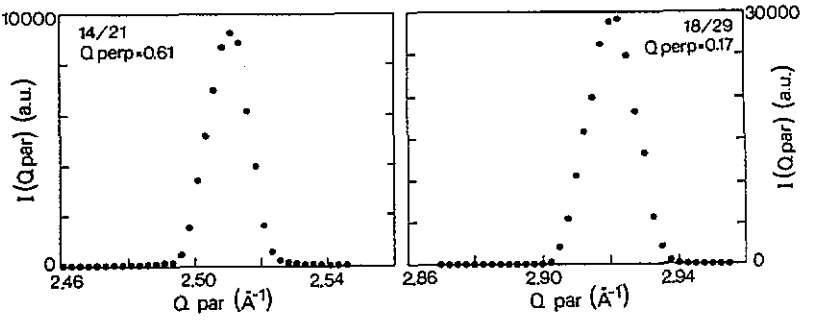

Figure 4. Elastic scan through two Bragg reflections with a large Q_{perp} difference. Peaks are resolution limited and do not show any Q_{perp} dependence.

We extend this calculation to the AlPdMn icosahedral phase, following the procedure used previously for electron density of state calculations [40, 41, 43, 44]. In 3D the starting structure could be that of pure Al, with the corresponding dispersion relation. This is justified because the alloy mainly contains Al atoms, and also because sound velocities in the AlPdMn icosahedral phase are found to be very close to that in pure Al. In the 3D case the reflection of a phonon with a wavevector q on a Bragg plane G occurs if the following relation is fulfilled:

$$2\boldsymbol{q} \cdot \boldsymbol{G} = \pm|\boldsymbol{G}|^2. \tag{7}$$

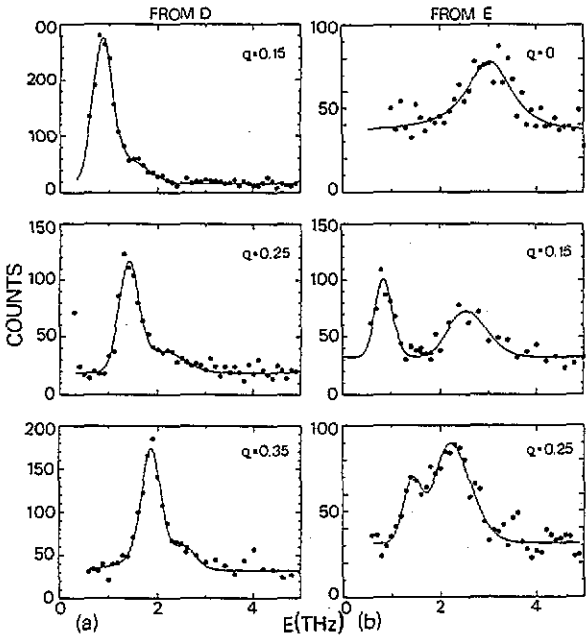

Figure 5. Constant-Q energy scans measured between points D and E. Points represent experimental data and the full curves are the results of the fit by a damped harmonic oscillator. (*a*) Starting from the Bragg D peak. The q value (taking D as origin) corresponding to each scan is indicated. The value q = 0.35 $Å^{-1}$ corresponds to the mid-point between D and E, i.e. to a pseudo zone boundary X_5. The main excitation has a width which is resolution limited. (*b*) Starting from the Bragg E peak. One can see both excitations coming from E (lower energy) and D. The q value, taking E as origin, is indicated.

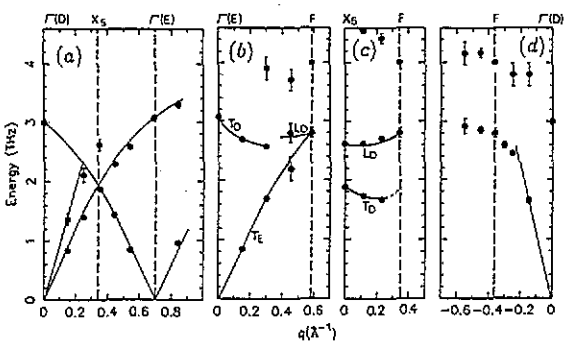

Figure 6. Dispersion relations around point D. The linear dispersion of transverse and longitudinal acoustic modes, according to ultrasonic sound velocity measurement, is shown as full straight lines in the figure. Broken lines are guides for the eye. (*a*) Dispersion between Γ point D and Γ point E: both acoustic branches originating from D and E can be followed. There is no visible gap when the two branches cross at X_5. (*b*) Dispersion between Γ point E and F which is an X_2 zone boundary point: the acoustic branch originating from E can be followed. The modes around 3 THz correspond to acoustic modes originating from D. These branches are labelled T_D and L_D on the figure, corresponding to transverse and longitudinal modes. There is a dispersionless optic mode around 4 THz. (*c*) Dispersion between X_5 and F: we mainly measure excitations originating from D. In X_5 we see mostly the transverse mode, whereas the longitudinal mode is seen in F. (*d*) Dispersion between D and F: the longitudinal mode becomes dispersionless rapidly. An optic mode around 4 THz is visible.

G is a vector of the quasiperiodic reciprocal lattice. The intensity of this gap is also proportional to the structure factor $F(G)$ [40,41]. However we have to take into account two effects: the quasiperiodicity and the introduction of Pd and Mn atoms with a mass significantly different to that of the Al. In calculating the structure factor this is roughly

taken into account by introducing weights inversely proportional to the square root of the mass of the different atoms. To locate the strongest gaps we define a general 'mass' structure factor F_m as

$$F_m(G) \propto \sum_{i=1}^{3} \frac{1}{\sqrt{m_i}} F_i(G) \tag{8}$$

where i is for the atom (Al, Mn or Pd) and F_i is the structure factor of the corresponding sublattice. G is a vector of the quasiperiodic reciprocal lattice. F_i is calculated using a model derived from neutron and x-ray single-crystal data [36]. The result of this calculation is presented in figure 2, in which the area of each spot is proportional to $F_m(G)$.

When only the strongest gaps are considered, the relation (7) defines a series of intersecting planes which can be named pseudo-Brillouin zone boundary. Starting from a zone centre there are three successive shells. They are represented in figure 2, around the origin chosen as the zone centre. The first pseudo-zone boundary is defined by the intersection between a triacontahedron and a dodecahedron: the two symmetry points which define this volume are X_5 on a fivefold axis and X_2 on a twofold axis, following the labelling of special points proposed by Niizeki and Akamatsu [43,44] (also see table 2). There is then a second shell defined by the intersection of an icosahedron and a dodecahedron (broken lines in figure 2), and finally the same volume, τ times larger, with special points L_5'' and L_3''. The associated Bragg peaks are stronger than for the previous volume, so that this is the second 'important' pseudo-zone boundary to be considered. Similarly to the 1D case, the upper limit to be considered is given by the pure Al zone boundary, i.e. $2q \simeq 2$ Å^{-1}. Gaps are expected to be evidenced easily in the low part of the 'dispersion relation', i.e. in the region where acoustic modes are still well defined. From the experimental point of view, this implies that the important zone centres are those corresponding to strong Bragg peaks, where acoustic modes are intense. Around each strong Bragg peak chosen as a zone centre there is thus a series of pseudo-zone boundaries. Each time the acoustic branch crosses such a zone boundary, a gap will open up and the dispersion relation will present a horizontal slope.

Table 2. Indices of the Bragg reflections corresponding to some of the special points of the pseudo-Brillouin zone (see figure 2). The position of the special point is given by $Q_{par}/2$. The last column indicates the value of $F_m(Q_{par})$ calculated with equation (1) (see text). Labels refers to those proposed by Niizeki and Akamutsu [43,44] all indices are given in the primitive unit cell [42].

Label	N	M	M_u	h/h'	k/k'	l/l'	n_1	n_2	n_3	n_4	n_5	n_6	Q_{par} (Å^{-1})	$F_m(Q_{par})$
X_5	2	1	12	1/0	0/1	0/0	1	0	0	0	0	0	0.689	1.0
X_2	4	0	30	2/0	0/0	0/0	1	0	0	−1	0	0	0.724	0.80
L_3'	3	3	20	1/1	1/0	0/0	0.5	0.5	0.5	−0.5	0.5	−0.5	1.015	0.72
L_5'	3	4	12	0/1	1/1	0/0	0.5	0.5	0.5	−0.5	0.5	0.5	1.114	0.30
L_3''	6	9	20	1/2	0/1	0/0	1	1	0	0	1	0	1.642	1.10
L_5''	7	11	12	1/1	1/2	0/0	0.5	1.5	0.5	−0.5	0.5	0.5	1.803	1.70

One may wonder what the difference would be between a quasicrystal (QC) and a periodic approximant. If we had the 1/1 cubic approximant to the AlPdMn system, the strongest Bragg reflections would be located at almost the same place in reciprocal space except for small distortions. The same series of important zone boundaries will thus be

defined, but now obviously periodically stacked. The corresponding Brillouin zones are distorted and do not show icosahedral symmetry, but strong gaps will be located at almost the same place. The only difference from the QC phase, in that respect, would be the sequence of gaps which is periodic in one case and quasiperiodic in the other case.

Finally, looking at figure 2, one also understands that a gap, if any, has very little chance to show up on the general vibrational density of states, since a spatial averaging is performed. The q position of gaps will change slightly, because the Brillouin zone is not a perfect sphere, leading to a smearing of the gap in the density of states.

To describe the experimental results we will adopt a simple classification. Since the term phonon has a clear meaning only in the acoustic regime, each strong Bragg peak is considered as a zone centre. Starting from these points, the dispersion relation is presented in an 'extended zone' scheme. Around each of these Γ points there is a series of quasiperiodically stacked pseudo-zone boundaries. The term 'pseudo-Brillouin zone' refers to the location of reciprocal space where strongest gaps are expected.

Along these lines phonon dispersion relations have been measured around several zone centres and along directions joining a Γ point to points X_5, X_2, L_5'' and L_3''.

3. Experimental details

The AlPdMn phase, discovered by Tsai *et al* [45, 46], can be obtained by slow cooling from the melt. A single grain of approximate size $1 \times 0.7 \times 0.5$ cm was obtained by the standard Bridgman growth technique [47]. Its composition was determined to be $Al_{68.7}Pd_{21.7}Mn_{9.6}$ [47]. Its quasicrystallinity and quality were checked by γ-ray and elastic neutron diffraction measurement. All of the sample diffracts, and no other phase was detected. The overall mosaicity is of the order of 0.8°, the sample being built up of about ten slightly misoriented subdomains each with a mosaic spread smaller than 0.1°. Figure 3 shows a typical Q scan taken along a fivefold axis. There is no phason strain in the sample since Bragg reflections exhibit resolution limited widths when measured by both elastic neutron scattering (figure 4) and high-resolution x-ray diffraction [47].

The sample was oriented to provide measurements in a twofold scattering plane which contains all the strong Bragg reflections (figure 1). Inelastic measurements were performed at the Orphée reactor of the Laboratoire Léon Brillouin, on the 1T triple-axis spectrometer with pyrolytic graphite (PG [002]) as monochromator (vertically bent) and analyser. First, constant-k_f scans (2.662 $Å^{-1}$) were carried out to measure phonons at room temperature, using either a flat or a bent analyser with an energy resolution of 0.35 THz. Tests made with silicon crystal showed that the resolution function obtained with the bent analyser was well accounted for by a pseudo-collimation of $43' \times 43'$, the signal being about twice that obtained with the flat analyser. Working with the bent analyser reduces the q resolution, but this was not an important issue in our experiment as will be shown in section 4. In a second step, similar to the procedure used with an AlCuFe sample [33], measurements were performed at 600 K with a bent analyser. This setting was used to look at high-energy excitations, where the signal is rather weak. A careful comparison of the results obtained at room temperature and at 600 K did not show any difference in the positions and widths of the excitations. Results of these measurements are presented in the following section.

4. Experimental results

4.1. Acoustic modes

In the acoustic regime well defined transverse and longitudinal excitations are measured (figure 5): the response function presents peaks whose width is limited by the instrumental resolution, and the correspondence between $S(Q,\omega)$ and the phonon dispersion curve is tracked out following expression (6). The linear character of the dispersion relation holds for q values up to 0.3 $Å^{-1}$ for transverse modes and up to 0.2 $Å^{-1}$ for longitudinal modes. In this region the measured acoustic excitations have a resolution limited energy width.

The isotropy of transverse and longitudinal modes propagating along different symmetry axes has been verified. Sound velocities were determined to be equal to $3.5(\pm0.1) \times 10^3$ m s^{-1} and $6.3(\pm0.3) \times 10^3$ m s^{-1} for transverse and longitudinal modes respectively. This was obtained by averaging eight different series of measurements for transverse modes propagating along two-, three-, and fivefold axes and three series of measurements for longitudinal modes propagating along two- and fivefold axes. This result is similar to those obtained for AlCuFe [32] and AlLiCu [30,31] quasicrystals. Note that the isotropy of acoustic modes was also observed in the crystalline R-AlLiCu phase [31]. These results are also in good agreement with ultrasound measurements made on the same AlPdMn sample [48]. The velocity of ultrasonic waves propagating along a twofold or a fivefold axis have been found to be $3593(\pm3)$ m s^{-1} for transverse modes and $6520(\pm10)$ m s^{-1} for longitudinal modes. In the ultrasonic experiment the isotropy was also checked to a precision of one part in 10^4 for waves propagating along a twofold direction with different polarizations.

Away from the acoustic regime the response function $S(Q,\omega)$ has been measured in various locations in reciprocal space. It will be seen in section 4.5 that the peaks broaden quite rapidly as the wavevector q increases. As we enter this region the relation between a phonon dispersion curve and the measured spectrum cannot be assessed simply. However, in order to parametrize experimental spectra, we have fitted the observed peaks with the response of a damped harmonic oscillator convoluted with the instrumental resolution. The background was found to be flat and fixed to a constant value for all scans ($\simeq$ 7 counts min^{-1}). Typical results of the fits obtained along the D–E line are presented in figure 5.

Having performed these fits, we may report the results in the form of a 'pseudo-dispersion' relation in an extended zone scheme. The various strong Γ points, and the special points at pseudo-zone boundaries discussed in section 2, are indicated on these graphs. In doing this one assumes that when going out of the acoustic regime the same zone centre may be used to define the wavevector q. This is partly justified by the continuity in the inelastic structure factor of the measured signal which has been experimentally observed (expression (6)). However, results should be discussed only in the term of the $S(Q,\omega)$ function to be completely rigorous. Finally since calculations on realistic 3D models are in progress, the presentation of the experimental results will be essentially descriptive.

We turn now to the presentation of the different dispersion relations measured in the twofold scattering plane. For the sake of simplicity, they are classified with respect to the strong Bragg peaks chosen as zone centres.

4.2. Dispersion relations around the Γ point D

The first region of interest is around the point D. This Bragg reflection is very strong and occurs at high G value, which means that acoustic modes are expected to be very strong

(expression (6)). Moreover there is a medium-intensity reflection E that is close, the D–E direction being parallel to a fivefold axis. The pseudo-zone boundary between points D and E corresponds to an X_5 point, a point where one of the strongest gaps is expected (see table 2 and figure 2): this region seems thus to be favourable to look for a gap in the dispersion relation.

When measuring acoustic phonons from D to E, q and Q are not orthogonal, so both the transverse and longitudinal acoustic modes propagating along a fivefold axis are measured (expression (6)): the longitudinal mode appears as a small shoulder in figure 5(*a*). Because of the relatively large crystal size, the acoustic mode associated with the Γ point E also gives a reasonable signal (figure 5(*b*)). The intensities of Bragg reflections D and E are in the ratio 10/1, in good agreement with the intensity ratio of corresponding phonons in the linear acoustic regime (expression (6)).

At the pseudo-zone boundary, where there is a crossing of the two acoustic branches, one would expect that a gap opens giving rise to an optic-like upper branch. At the X_5 point ($q = 0.35$ Å^{-1}, figure 5(*a*) the measured excitation is still resolution limited (0.3 THz) and no such gap was actually detected. This means that a gap, if any, must have an energy width lower than 0.15 THz.

However both acoustic branches can be followed after their crossing. In particular the signal associated with the Bragg D peak gives still a very clear contribution, even above the Γ point D (figure 5(*b*), top panel). One has thus a situation where an acoustic mode and an excitation at higher energy coexist (figure 5(*b*), $q = 0.15$ Å^{-1} for instance). When such a situation occurs in a crystal, the upper branch is no longer an acoustic branch and must be called optic. In that sense, we have measured an 'optic' mode, but its labelling is obviously not possible.

The corresponding dispersion curves are presented in figure 6. Note that the present result is different to what was observed in the i-AlLiCu phase [31]. In that case the dispersion relation presents a maximum at the pseudo-zone boundary, with no other mode above the acoustic branch, in contrast to what is observed here.

The response function was then measured along the line E–E′ (E′ is the mirror image of E), corresponding to phonons propagating along the twofold direction. The distance between Bragg reflections is τ times larger than for D–E. Since there is a mirror plane at the mid point of E–E′ (denoted F) only half of the dispersion relation has been measured, the other half being deduced by symmetry. Here again one can follow the acoustic mode up to the pseudo-zone boundary.

Around 3 THz there seems to be a slightly dispersive optic branch. In fact other measurements in this area showed that these modes could be well accounted for by acoustic phonons associated with the strong Bragg reflection D. When going from E to F, because of the scalar product $e_{T(L)} \cdot Q$ (expression (6)) the relative contribution of transverse and longitudinal modes will change in the response function $S(Q, \omega)$. In E the main contribution is given by the transverse acoustic mode whereas in F the transverse acoustic mode makes no contribution to the signal and the longitudinal mode has a maximum intensity (in F, q and Q are parallel). These two branches are indicated by the labels L and T in figure 6.

This interpretation was confirmed by measurements made between the X_5(D–E) pseudo-zone boundary and F (figure 6). The notation X_5(D–E) refers to the pseudo-zone boundary located between the Bragg peaks D and E. When going from X_5(D–E) to F the transverse mode associated with the Γ(D) point decreases in intensity and goes to zero, while the longitudinal mode becomes more intense. The relative intensity variation is in good agreement with the variation of the scalar product $e_{T(L)} \cdot Q$.

In the E–F region an optic mode, lying at 4 THz and dispersionless, is also measured.

Finally, longitudinal modes were measured starting from D in the direction of F (figure 6) thus completing a loop in this region of the reciprocal space. The dispersion curve clearly bends over around 3 THz. An optic mode, which is non-dispersive and lying around 4 THz, has also been identified. Moreover, the longitudinal acoustic phonon broadens quite rapidly, when its energy exceeds about 2 THz. Above that energy, excitations become so broad that the description in term of a damped harmonic oscillator is probably no longer appropriate. The observed lineshape could be accounted for using two oscillators. A more complete study of mode broadening will be presented in section 4.5 for transverse modes, where the energy resolution is better when working in the focusing geometry.

This longitudinal dispersion curve along D–F is comparable to the measurements in the i-AlLiCu phase [31], for which longitudinal modes become dispersionless though at a lower energy (i.e. around 2.5 THz). This was at variance with the behaviour observed in the approximant crystalline R phase and was interpreted as an indication of spatial localization of the corresponding 'phonon modes' in the quasicrystal. In effect, if spatial localization of modes occur, this leads to a non-dispersive branch.

Figure 6 gathers all results in the area D–E–F. The different acoustic and optic branches are easily traced out, when going from one direction to the other. At pseudo zone boundaries there is no evidence for gaps, even when branches cross. The picture which emerges from the study in this area is that there is a series of excitations, with a pronounced acoustic character (see the effect of $e \cdot Q$), associated with two distinct Γ points (D and E) and which have an 'independent' behaviour, i.e. which do not 'interact'. In some regions there is a clear dispersionless optic mode located at 4 THz. When measuring the response function in other regions of the reciprocal space we will see that the situation is similar.

4.3. Dispersion relation around the Γ point A

Longitudinal and transverse modes were measured around the Bragg reflection A. In both cases the situation is quite similar to measurements made around point D.

For longitudinal modes, going in the direction of the weak reflection B, one can measure two excitations: one corresponding to the longitudinal acoustic mode which becomes dispersionless around 3 THz, and an optic mode around 4 THz. Data and the corresponding dispersion curve are shown in figure 7 and figure 8. As can be clearly seen in figure 7, the longitudinal acoustic mode broadens when it reaches an energy of about 2 THz. At the same time its dispersion relation is no longer linear, and tends rapidly towards a dispersionless excitation with an energy of 3 THz. At the same time a higher-energy optic mode located around 4 THz shows up. At higher momentum transfer, the excitations merge, and their separation becomes difficult.

This 4 THz optic mode was mainly observed in 'longitudinal' geometry, i.e. between D and F and between A and B. Note that the identification of this mode as longitudinal is tentative, because one needs to associate this excitation to a given zone centre in order to define the wavevector q properly. This can be done without ambiguity only for acoustic modes. If we suppose that the zone centre associated with this excitation is A, i.e. that the corresponding wavevector can be written $q = Q - G(\mathrm{A})$, then from relation (4) one can deduce that this optic mode should have mainly a 'longitudinal' character, i.e. its pattern of atomic displacements is mainly parallel to the wavevector. But once again we point out the difficulty of interpreting the experimental results!

Transverse mode measurements of phonons propagating in the $[-\tau, 1, 0]$ direction show a smooth bending, similar to the transverse D mode (figure 12(e)).

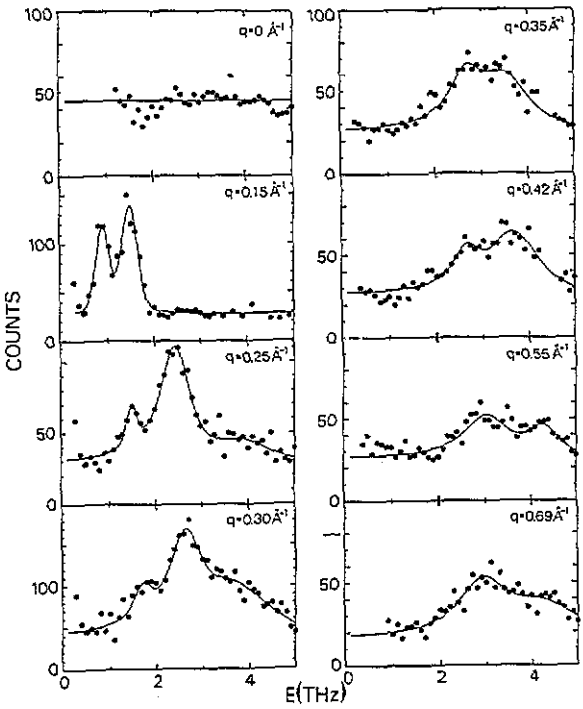

Figure 7. Constant-Q scans measured between points A and B. Points represent experimental data and the full curves are the result of the fit with a damped harmonic oscillator. Because of the relaxed out-of-plane resolution, both the transverse and the longitudinal acoustic modes show up. Notice the rapid broadening of the longitudinal excitation for q larger than 0.2 Å^{-1}. An optic mode, located around 4 THz, also shows up clearly.

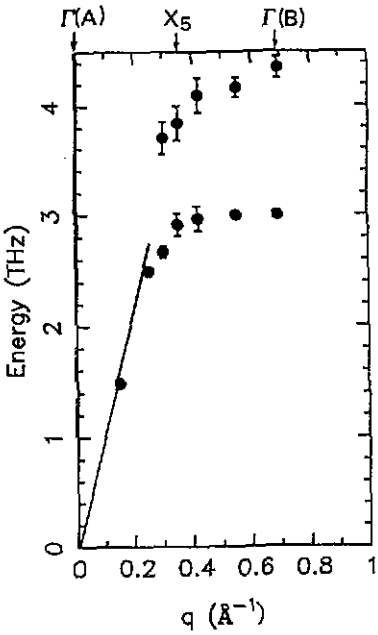

Figure 8. Phonon dispersion relation along the direction A–B. The full line corresponds to the linear dispersion relation according to ultrasonic sound velocity measurements. The acoustic longitudinal mode, propagating along the fivefold direction, bends over rapidly. This is to be compared to results obtained for longitudinal modes propagating along the twofold axis (figure 6(*d*)). An optic mode lying around 4 THz is measured in both cases.

4.4. Dispersion relation around the Γ point D′

The point D′ is the symmetry equivalent of point D. In this region, two strong Bragg reflections, G and H, may give measurable acoustic modes. The directions D′–G and D′–H

are parallel to a threefold axis. The pseudo-zone boundary corresponds to an L_3'' special point. The dispersion relations are presented in figure 9. Both the longitudinal and the transverse acoustic modes propagating along a twofold axis are measured.

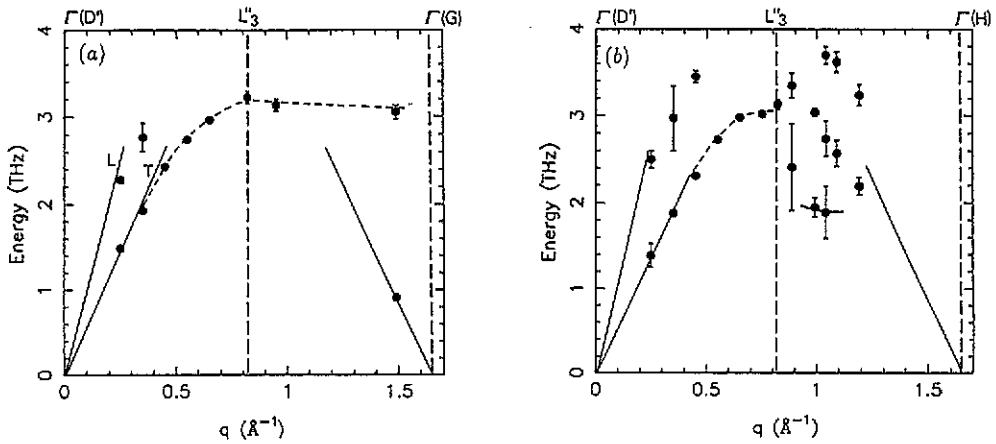

Figure 9. (*a*) Dispersion relation along the direction D′–G. The acoustic transverse mode, originating from D′, bends over in the 3 THz energy range. No gap is visible at the zone boundary L_3''. (*b*) Dispersion relation along the direction D′–H. The left part of the dispersion relation is similar to figure 9(*a*). In the right part (L_3''–H) two or three modes are measured. The low-energy mode around 2 THz is an acoustic branch arising from an out-of-plane Bragg reflection. Some of the data and results of the fit are shown in figure 10.

Along the direction D′–G, the transverse acoustic branch can be followed up to the Γ point G (figure 9(*a*)). There is a pronounced bending of the dispersion curve when the mode reaches an energy of 3 THz: for this energy the mode becomes dispersionless. At the zone boundary point (L_3''), the response function was still fitted by a single excitation, although this one is already relatively broad (phonon width 1 THz). Similar to what was observed in other regions, the inelastic structure factor deduced from the measured integrated intensity is almost constant for all q values. This justifies, *a posteriori*, the presentation of the results in the form of a 'dispersion relation'.

Measurements along the direction D′–H were performed at a final energy $k_f = 3.85$ Å^{-1} to allow the high-Q region of this scan to be reached. With this setting the energy resolution is only about 1 THz. Since the resolution ellipsoid is much larger, intensities are collected from a large region in the (Q, ω) space and caution must be taken to analyse the data. Results of the measurement are presented in figure 9(*b*). In the region D′–L_3'' the picture is quite similar to that previously described: there is an acoustic longitudinal mode and a transverse acoustic mode propagating along the threefold axis. The transverse acoustic mode bends over when reaching the 3 THz energy region, similarly to what is observed in figure 9(*a*). The situation in the L_3''–H region is more complex. After the special point L_3'' at least two, and then three, excitations are necessary to describe the measured response function. There is a low-energy mode around 2 THz which is probably related to a relatively strong Bragg reflection lying above the plane at a distance of 0.5 Å^{-1}. When passing close to this peak the associated longitudinal acoustic mode shows up. The medium-energy excitation is related to the transverse acoustic mode associated with H, and the upper optic mode at 3.5–4 THz may probably be seen as a 'continuation' of the transverse branch originating

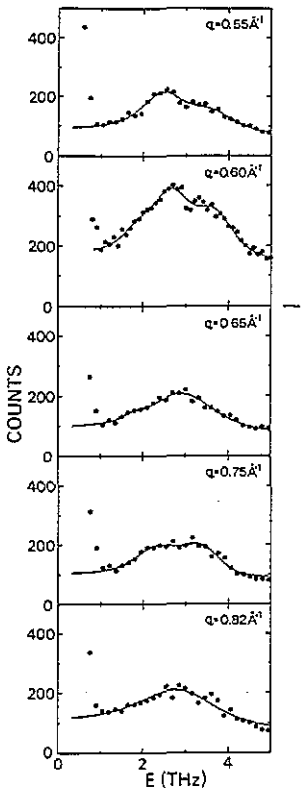

Figure 10. Constant-q scan, taken in the L_3''–H region. The distance q is by reference to the Γ point H. The full curves are the result of a fit with several damped harmonic oscillators. The corresponding result of the fit can be seen in figure 9(*b*). Note the 'window'-like shape of the excitation at $q = 0.75$ Å^{-1}.

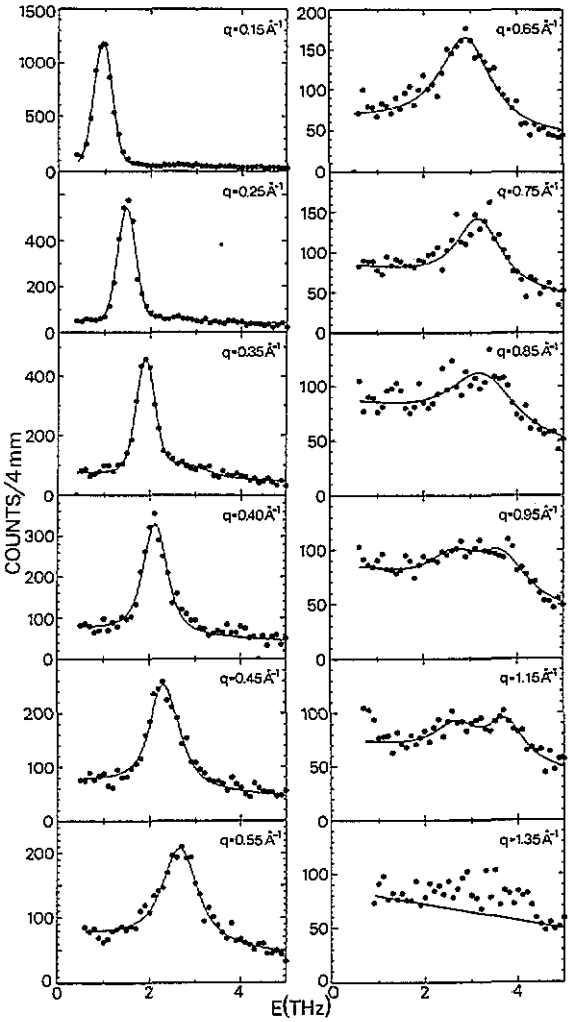

Figure 11. Transverse phonons measured from the Γ point D. Points are experimental results and full curves refer to a fit with a damped harmonic oscillator. There is a broadening of the phonon starting at $q = 0.4$ Å^{-1}. In the high-energy region (above $q = 0.85$ Å^{-1}), two excitations are necessary to describe the data.

from D′. What is clear, as can be seen in figure 10, which shows some of the data taken in this area, is that there are several contributions.

4.5. Broadening of transverse modes

A careful study of the widths of the measured excitations has been undertaken in the purely transverse geometry starting from points D and D′. As previously mentioned, the experimental results were fitted with a damped harmonic oscillator convoluted with the

and for measurement of transverse modes in the focusing geometry, the instrumental energy width is smaller than 0.3 THz.

Figure 11 shows the experimental results for transverse modes measured from point D. The result of the fit is indicated by full curves. In the low-energy region the measured phonon has a width which is limited by the instrumental resolution and the dispersion relation is linear. From $q = 0.4$ Å^{-1} there is a clear broadening of the excitation. The linewidth of the phonon increases rapidly up to $q = 0.7$ Å^{-1} where it reaches a constant value of 1 THz. From $q = 0.95$ Å^{-1} the observed signal has been accounted for by two modes each with a width equal to 1 THz (see also figure 13(*a*)). Attempts to fit this signal with only one contribution gave a significantly worse result. Similar measurements were made starting from D′. The positions of phonons together with their respective widths (after deconvolution from instrumental resolution) are reported in figure 12(*a*) and (*b*). In both cases the full width at half maximum (FWHM) increases rapidly between $q = 0.4$ Å^{-1} and $q = 0.7$ Å^{-1} and reaches an unusually large value of 1 THz. However the response function presents significant differences for q larger than 0.95 Å^{-1}. Whereas at least two phonons have to be considered in order to reproduce the signal observed in the D region, the response function in the D′ region still can be accounted for by a single broad phonon (1 THz width). This is illustrated in figure 13 where both constant-$q = 0.95$ Å^{-1} scans are shown: the D response function presents a plateau with relatively steep fall-off, reminiscent of a continuous distribution, whereas the signal in the D′ region still has a Lorentzian shape and is well accounted for by a single phonon. Note also the difference in intensity: after background subtraction the maximum number of counts is about twice as large for the mode originating from D′ than for the one originating from D. This result may seem puzzling since D and D′ are equivalent twofold reflections. However, symmetry requirements do not impose the dispersion relation to be identical: this is because there is only a twofold symmetry axis and not a fourfold axis. In other words, it is not equivalent to look at the atomic structure along a twofold X axis and along a twofold Y axis. Regardless, the notion of dispersion relation becomes inappropriate in this region, and the only quantity to be considered is the response function: there is no reason why this quantity should be identical to both places.

In order to check for anisotropy of this broadening, we also measured transverse modes propagating along other symmetry directions. Interestingly, anisotropy in the attenuation of sound waves was observed in measurements made on the same sample [48]. This was interpreted as resulting from a phonon–phason coupling. Therefore it is interesting to check whether such an anisotropy occurred for the observed phonon broadening. All results show the same feature: the low-energy acoustic modes are resolution limited, and a rapid increase of the FWHM occurs around $q = 0.4$ Å^{-1}. No anisotropy could be detected. The results are shown in figure 12(*c*)–(*e*).

Results for transverse phonons propagating along a fivefold [1, τ, 0] direction and associated with the Γ point D are shown in figure 12(*c*). This direction is the mirror image of the D–E direction (figure 1) and $q = 0.35$ Å^{-1} is a special point of the Brillouin zone labelled X_5. In contrast to figure 6 where two acoustic branches, associated with Γ points D and E, cross, only one branch originating from D is measured in figure 12(*c*), because there is no other strong Bragg spot in this region (see figure 1). This might have been a more favourable experimental situation to observe a gap, but similar to what is observed in figure 6, no gap was detected. Figure 12(*d*) shows the position and FWHM of phonons propagating along a threefold axis along the direction D′–G. Finally, figure 12(*e*) shows the position and FWHM of phonons propagating along a [$-\tau$, 1, 0] direction from the point A. In all cases a rapid broadening occurs around $q = 0.4$ Å^{-1}. A similar broadening

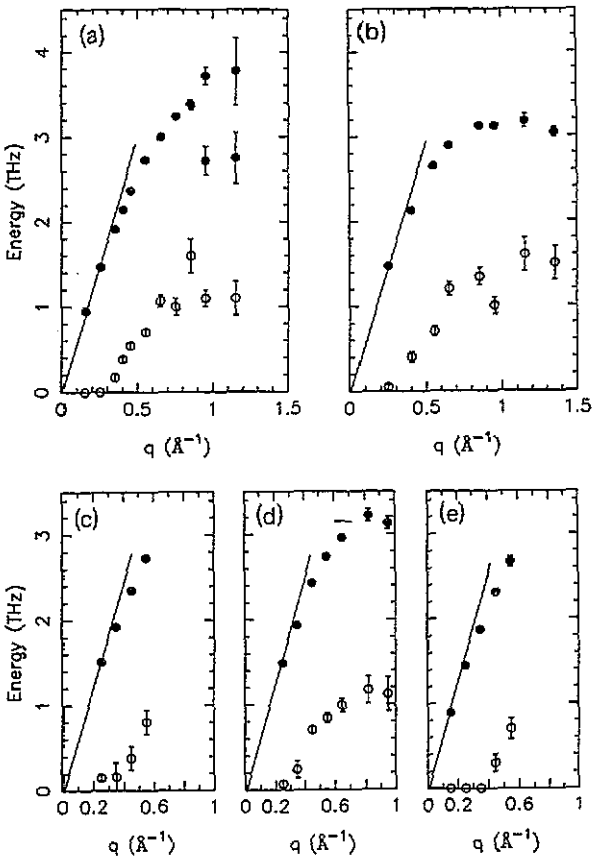

Figure 12. Dispersion relation and phonon width for transverse modes propagating in different directions: filled circles, phonon frequency; open circles, phonon width. The full straight lines correspond to the linear acoustic dispersion deduced from ultrasonic sound velocity measurements. For all directions there is a jump in the phonon width at around $q = 0.4$ Å^{-1}. (*a*) Transverse mode propagating along a twofold axis and measured from D. (*b*) Transverse mode propagating along a twofold axis and measured from D′. Notice the difference between (*a*) and (*b*) at high energy. (*c*) Transverse modes propagating along a fivefold axis measured from D, in the [1, τ, 0] direction. This direction is the mirror image of the D–E direction. (*d*) Transverse modes propagating along a threefold axis measured from D′ along the direction D′–G. (*e*) Transverse modes, propagating along the [$-\tau$, 1, 0] direction measured from A.

of one transverse mode was previously reported in the AlCuFe icosahedral phase [33].

What is the origin of such a large broadening? Two quite different processes can lead to the same experimental result. On one hand, the broadening may result from the finite lifetime of the excitation, and the picture of the damped harmonic oscillator is a good approximation. This could be the result of anharmonicity or could simply reflect the difficulty for plane waves to propagate in a quasiperiodic medium. On the other hand the broadening can result from the superposition of several modes. One can imagine that there is a continuum of dispersionless modes which would then be picked up in the measurement. In this case modes do not need to be damped; it is only the superposition of modes which give rise to the broadening. The very broad distribution that was measured for the higher-energy scans seems to be in agreement with the hypothesis of a continuous distribution. This picture is similar to what has been calculated in the 1D case by Benoit *et al* [19], where for high energy a large number of modes spread over a noticeable range in energy show up in the response function $S(\boldsymbol{Q}, \omega)$. Moreover a recent calculation performed by Poussigue *et al* [28] on an AlMn quasicrystal model shows that the icosahedral phase presents critical modes which form a continuum and lead to a broadening of the response function. The same calculation performed on a small approximant does not show the same broadening. The broadening we have experimentally observed is thus likely to be a signature of the quasicrystalline order.

The situation is summarized in figure 14. In the low-energy part we have well defined

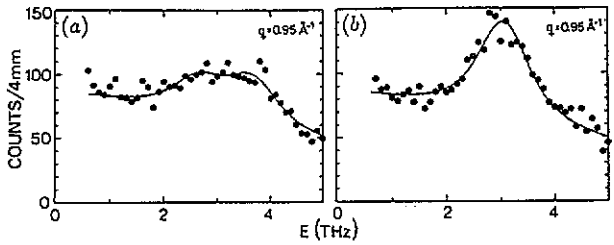

Figure 13. Comparison of the transverse mode measured at $q = 0.95$ Å^{-1} from D (a) and from D′ (b). There is a clear difference: two phonons are necessary to fit the data in (a), whereas only one phonon is visible in (b). The maximum intensity is also much larger in (b).

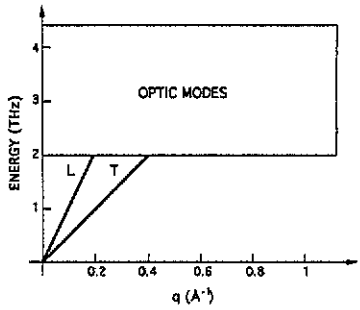

Figure 14. General picture of the distribution of modes in the i-AlPdMn phase. At low energy acoustic modes are well defined and do not present any width. There is a continuous distribution of optic modes in the range 2–4.5 THz. When a phonon is measured in this region it is broad.

acoustic phonons, with a long lifetime. In the region 2–4.5 THz, there is a continuum of optic modes. These modes do not show any dispersion and are localized. When the acoustic branch enters the 'sea' of optic modes, there is an interaction between the acoustic mode and the localized modes. This could be for instance anticrossing effects, which would result in a broadening of the response function $S(Q, \omega)$, each time the acoustic branch crosses an optic one [39]. An important point to notice is that the excitations we measured in this area still have an 'acoustic' character. In effect the intensity of the response function is still related to the intensity of the elastic structure factor of the Bragg reflection with which the excitation may be associated. Measurements performed in regions of the reciprocal space far from strong Bragg peaks do not show any signal except the background, which indicates that expression (6) still holds, although we are no longer in the linear regime. As a consequence, the wavevector q used in the pseudo-dispersion relation is probably still appropriate in this intermediate range.

The wavevector of the phonons for which this broadening occurs is of the order $q = 0.5$ Å^{-1} corresponding to a wavelength of about 12 Å. Interestingly enough, this is the same wavelength for which differences between the crystalline and the icosahedral phase were observed in the AlLiCu system. As was poinnted out by Goldman *et al* [31], this distance corresponds to the inter-cluster distances in AlLiCu phases. This is also the case here, and 12 Å is a typical inter-Mackay icosahedron distance along a twofold axis [36]. The quasiperiodic stacking of these clusters may be at the origin of the localization of the modes and their broadening.

On the other hand, if one takes the picture of the damped harmonic oscillator in the region where the broadening starts, one also can have some indication of the important length scale. We consider the situation where transverse phonons start to broaden and reach a width equal to 0.5 THz. In this region, one still has well defined phonons whose group velocity is given by $d\omega/dq$, i.e. by the local slope of the dispersion relation: it is of the order of 2000 m s^{-1}. A width of 0.5 THz corresponds to a lifetime t of the order of 0.3×10^{-12} s, to which is associated a characteristic length of the order of 6 Å, i.e. the

same order of magnitude as the one discussed previously. These are both strong indications that the basic structural elements that have to be considered when the broadening occurs have a size of order 10 Å: this is precisely the size of the Mackay icosahedron and of their intercluster distances. They constitute 60% of the AlPdMn structure.

Finally, it is interesting to compare the obtained dispersion relation with the integrated phonon density of states measured by Suck [49] on a powder AlPdMn sample with a time of flight spectrometer. These are two main contributions in the measured density of state: one that is relatively narrow and has a maximum for an energy equal to 4.1 THz, and another which is broad and centred around $E = 7$ THz. The optic mode, which is measured in various places and lies around 4 THz, is in agreement with the lower peak in the experimental density of states. However attempts to measure higher-energy modes were unsuccessful: measurements performed in various regions of the reciprocal space did not show anything except a flat background in the region 5–8 THz. This is probably because in this region the modes are localized and spread over reciprocal space; the spatially averaged measurement performed on a time of flight instrument allows one to collect data with a greater statistical accuracy than using a triple-axis spectrometer.

5. Conclusion

The dynamical properties of the icosahedral AlPdMn phase have been measured by inelastic neutron scattering on a single grain.

In the long-wavelength limit there are well defined phonons whose width is limited by the instrumental resolution. As for other icosahedral phases, the isotropy of accoustic modes in i-AlPdMn has been verified. The corresponding sound velocities are in good agreement with ultrasonic measurements performed on the same sample. This is the only region where the link between the measured response function and a given 'phonon branch' may be made without ambiguity.

At higher wavevector one would expect the opening of gaps. The regions where the strongest gaps are expected have been estimated using a perturbative approach and the known atomic structure. This defines a succession of pseudo-Brillouin zone boundaries which are quasiperiodically stacked. In principle all Bragg reflections may be chosen as zone centres, but only the strongest ones are of importance.

Attempts to observe such gaps at various points of the reciprocal space were unsuccessful. Even when two branches cross, no gap could be measured. This means that gaps, if present, have energy widths lower than 0.15 GHz.

Rigorously speaking it is no longer possible to discuss a dispersion relation outside the acoustic regime. However in the present experiment, all the measured signals could be associated with a relatively strong Bragg reflection, since the inelastic integrated intensity scales as the elastic Bragg peak intensity. This leads to a natural choice of these reflections as zone centres and allows the description of the results in term of 'dispersion relations'. This statement is probably only valid in an intermediate range. The general trends of the measured response function may be summarized as follows.

For 'longitudinal' polarization, the acoustic mode broadens quickly, when it reaches an energy of about 2 THz. At the same time the dispersion no longer shows a linear character, but bends over rapidly towards a 3 THz value where it becomes dispersionless. A well defined excitation, which is dispersionless, also shows up at an energy of 4 THz. Since this excitation does not show up in the transverse geometry, we assign it a 'longitudinal optic' label. For higher wavevectors these excitations merge to form a continuum.

For 'transverse' polarization and for wavevectors lower than 0.8 $Å^{-1}$ the behaviour of the response function is similar when observed around several strong Bragg peaks and for various directions of the wavevector. Starting from $q = 0.35$ $Å^{-1}$ the measured phonon broadens rapidly and its width reaches a value of 1 THz. This broadening has been found to be isotropic. At the same time the dispersion relation departs significantly from a linear behaviour and bends over.

At higher wavevector, i.e. $q > 0.8$ $Å^{-1}$, the response function with a transverse 'polarization' shows significant differences depending on location in reciprocal space. Two quite different behaviours have been observed. In one case the response function can be fitted by a single broad excitation (1 THz FWHM) up to a q value of 1.4 $Å^{-1}$. The energy of this excitation reaches a maximum of 3 THz at which value the excitation becomes dispersionless. In the other case, the response function continues to broaden and at least two excitations, each with a 1 THz width and centred on 2.7 and 4 THz, are necessary to describe the data.

We interpret these results as the consequence of an almost continuous distribution of dispersionless modes in the range 2–4.5 THz. This picture is summarized in figure 14. For the low-energy part we have well defined acoustic longitudinal and transverse modes. When these modes enter the 'sea' of optic modes (shaded area), an interaction between optic and acoustic modes occurs, which give rise to the broadening of the measured excitation. At higher q this region may be split in two 'optic bands', centred on 3 and 4 THz. Depending on the polarization and on the location in reciprocal space one or both of these bands are active.

It is interesting to compare these results to available data. At one extreme of the spectrum of atomic structures, we have the simplest crystalline structure which is the pure FCC Al. Its dispersion relations have been extensively measured [50]. In the long-wavelength limit it is interesting to note that both longitudinal and transverse sound velocities have almost the same values as those of the icosahedral phase. There are two different acoustic transverse modes but the difference between the sound velocities of these two modes is weak and drawing the Al dispersion curves on figure 14 would perfectly match the results (this is hopefully not the case with the high precision obtained in the ultrasonic measurements). At shorter wavelength, the phonon width is one order of magnitude smaller than in the icosahedral phase. There is almost no dependence of this width on the wavevector. The dispersion relation is also quite different: the bending of the dispersion relation occurs at a much higher energy and the region 0–4 THz the dispersion relation of pure Al departs only slightly from the linear regime.

At the other extreme of the spectrum we have the amorphous metallic materials. In this case [51] and for wavevectors accessible with neutrons, the excitations are very broad even for small wavevectors. Moreover, since there is no long-range order, measurements can only be performed close to the origin, and dispersion relations do not have a clear meaning.

In between we find the disordered alloys. In these systems, an atom is located at random on a periodic (in general simple) host lattice. The introduction of this disorder breaks the periodicity and gives rise do diffuse scattering in the diffraction pattern. However there are still Bragg peaks, since we have an underlying lattice [52]. There might be some similarities with the problem of quasicrystals, although we emphasize once again that quasicrystals are highly ordered long-range structures. Because of the mass defects in these disordered systems, local modes are present. This shows up in the response function, which presents a broadening of the excitations when one goes outside the acoustic regime. The final broadening is comparable to what is observed here (i.e. of the order of 1 THz), but there is more structure as a function of q. Moreover, the energy positions of these

excitations follows closely the dispersion curve of the pure host crystal and do not present a dispersionless character, in contrast to the icosahedral case.

We believe that the results we have obtained in the i-AlPdMn phase are a characteristic feature of the icosahedral state. The picture we propose (figure 14) is in agreement with the 1D calculation performed by Benoit *et al* [19], and also with more recent calculations performed on a realistic 3D model [28]. This is also compatible with the results obtained by Los *et al* [26], where the calculated dispersion relations show a large number of optic modes in the high-energy region.

When the broadening of the acoustic modes begins, both the width of the phonon and the wavelength of the wavevector indicate that the characteristic atomic length scale involved is of the order of 10 Å. This is precisely the size of the Mackay icosahedron and intercluster bound length. It has been shown that such clusters do exist in the AlPdMn phase and are hierarchically packed. The hierarchical and quasiperiodic packing of these clusters might be at the origin of the localization of the phonons.

The interpretation of the present experimental results is only very tentative and needs to be confirmed by more detailed calculations on a realistic atomic model. This is in progress.

Acknowledgments

The Laboratoire Léon Brillouin is a Laboratoire Commun CEA-CNRS. We thank the staff at the Laboratoire Léon Brillouin for technical support. Fruitful discussions with G Poussigue, C Benoit, J Los, F Gähler, T Janssen, J B Suck and L Levitov are acknowledged.

References

[1] Guyot P, Kramer P and de Boissieu M 1991 *Rep. Prog. Phys.* **54** 1373
[2] Goldman A I and Widom M 1991 *Am. Rev. Phys. Chem.* **42** 685
[3] Janot C 1992 *Quasicrystals: a Primer* (Oxford: Oxford University Press)
[4] De Lange C and Janssen T 1981 *J. Phys. C: Solid State Phys.* **14** 5269
[5] Ashraff J A, Luck J M and Stinchcombe R B 1990 *Phys. Rev.* B **41** 4314
[6] Ostlund S, Pandit R, Rand D, Schellenhuber H J and Siggia E D 1983 *Phys. Rev. Lett.* **50** 1873
[7] Kohmoto M, Kadanoff L P and Tang C 1983 *Phys. Rev. Lett.* **50** 1870
[8] Ostlund S and Pandit R 1984 *Phys. Rev.* B **29** 1394
[9] Luck J M and Petritis D 1986 *J. Stat. Phys.* **42** 289
[10] Lu J P, Odaki T and Birman J L 1986 *Phys. Rev.* B **33** 4809
[11] Tamura S and Wolfe J P 1987 *Phys. Rev.* B **36** 3491
[12] Kohmoto M, Sutherland B and Tang C 1987 *Phys. Rev.* B **35** 1020
[13] Lu J P and Birman J L 1987 *Phys. Rev.* B **36** 4471
[14] Lu J P and Birman J L 1988 *Phys. Rev.* B **38** 8067
[15] Janssen T and Kohmoto M 1988 *Phys. Rev.* B **38** 5811
[16] Patel H and Sherrington D 1989 *Phys. Rev.* B **40** 11 185
[17] Levitov L S 1989 *J. Physique* **50** 707
[18] Ashraff J A and Stinchcombe R B 1989 *Phys. Rev.* B **39** 2670
[19] Benoit C, Poussigue G and Azougarh A 1990 *J. Phys.: Condens. Matter* **2** 2519
[20] Benoit C 1989 *J. Phys.: Condens. Matter* **1** 335
[21] You J Q, Yand Q B and Yan J R 1990 *Phys. Rev.* B **41** 7491
[22] Currat R and Janssen T 1988 *Solid State Phys.* **41** 201
[23] Janssen T 1988 *Quasicrystalline Materials* ed C Janot and J M Dubois (Singapore: World Scientific) p 327
[24] Ashraff J A, Luck J M and Stinchcombe R B 1990 *Phys. Rev.* B **41** 4314
[25] Los J and Janssen T 1990 *J. Phys.: Condens. Matter* **2** 9553
[26] Los J, Janssen T and Gähler F 1992 *J. Non-Cryst. Solids* to appear; 1993 *J. Physique* **3** 107
[27] Hafner J and Krajci M 1993 *Europhys. Lett.* **21** 31

[28] Poussigue G, Benoit C, Azougarh A, de Boissieu M, Currat R and Janot C 1992 *SFP meeting (Lille, 1992)* and in preparation
[29] Kasner G and Bötger H 1992 *J. Non-Cryst. Solids* at press
[30] Goldman A I, Stassis C, Bellissent R, Moudden H, Pyka N and Gayle F W 1991 *Phys. Rev.* B **43** 8763
[31] Goldman A I, Stassis C, de Boissieu M, Currat R, Janot C, Bellissent R, Moudden H annd Gayle F W 1992 *Phys. Rev.* B **45** 10280
[32] Quilichini M, Heger G, Hennion B, Lefebvre S and Quivy A 1990 *J. Physique* **51** 1785
[33] Quilichini M, Heger G, Hennion B, Lefeovre S and Quivy A 1992 *J. Physique* II **2** 125
[34] Cornier-Quiquandon M, Quivy M, Lefebvre S, Elkaim E, Heger G, Katz A and Gratias D 1991 *Phys. Rev.* B **44** 2071
[35] Boudard M, de Boissieu M, Janot C, Dubois J M and Dong C 1991 *Phil. Mag. Lett.* **64** 197
[36] Boudard M, de Boissieu M, Janot C, Heger G, Beeli C, Nissen H-U, Vincent H, Ibberson R, Audier M and Dubois J M 1992 *J. Phys.: Condens. Matter* **4** 10149
[37] de Boissieu M, Janot C, Dubois J M, Audier M and Dubost B 1991 *J. Phys.: Condens. Matter* **3** 1
[38] Lovesey W L 1984 *Theory of Neutron Scattering from Condensed Matter* (Oxford: Clarendon)
[39] Dorner B 1982 *Coherent Inelastic Neutron Scattering in Lattice Dynamics* (Berlin: Springer)
[40] Smith A P and Ashcroft N W 1987 *Phys. Rev. Lett.* **59** 1365
[41] Friedel J and Denoyer F 1987 *C. R. Acad. Sci., Paris* **305** 171
[42] Cahn J W, Shechtman D and Gratias D 1986 *J. Mater. Res.* **1** 13
[43] Niizeki K 1989 *J. Phys. A: Math. Gen.* **24** 4295
[44] Niizeki K and Akamatsu T 1990 *J. Phys.: Condens. Matter* **2** 2759
[45] Tsai A P, Inoue A, Yokoyama Y and Masumoto T 1990 *Mater. Trans. JIM* **31** 98
[46] Tsai A P, Inoue A and Masumoto T 1990 *Phil. Mag. Lett.* **62** 95
[47] de Boissieu M, Durand-Charre M, Bastie P, Carabelli A, Boudard M, Bessiere M, Lefebvre S, Janot C and Audier M 1992 *Phil. Mag. Lett.* **65** 147
[48] Amazit Y, de Boissieu M and Zarembovitch A 1992 *Europhys. Lett.* **20** 703
[49] Suck J B 1993 *J. Non-Cryst. Solids Proc. 4th Int. Conf. on Quasicrystals* **153 & 154** 573
[50] Stedman R and Nillson G 1966 *Phys. Rev.* **145** 492
[51] Suck J B 1992 *J. Non-Cryst. Solids* at press
[52] Taylor D W 1982 *Excitations in Disordered Systems* ed M F Thorpe (New York: Plenum) p 297 and references therein